Absolute hadron beam polarimetry at EIC

Frank Rathmann
Brookhaven National Laboratory

20th International Workshop on Polarized Sources, Targets, and Polarimetry
Jefferson Lab, Newport News, Virginia

September 24, 2024

Initial observation

- In recent years, many groups specializing in **polarization instrumentation & technology** for hadronic probes have disappeared, along with the valuable expertise they once contributed. This contrasts sharply with the time when RHIC was conceived, when numerous experimental and theoretical groups from around the world provided a wealth of expertise.
- Currently, we face a critical situation, with a shortage of skilled individuals, which is crucial to overcome for the EIC's success.
- There is an urgent need to rejuvenate polarization instrumentation & technology for hadrons and expand education and training efforts.[1].

[1] Key areas are highlighted in https://technotes.bnl.gov/PDF?publicationId=225693

Contents I

Hadron polarimetry requirements for the EIC I

Comments

- The EIC will use polarized **protons** and **helions**, later on possibly deuterons, and heavier nuclei like lithium may be needed
- **The EIC promises to provide proton beam polarizations over 70% with a relative uncertainty of 1% or better**
- **Absolute beam polarization relies on precisely measured nuclear polarization of an atomic jet**
  - Elastic scattering of identical particles, like in $\vec{p}\vec{p}$ scattering
  - Polarization calibration needed for each ion species ($\vec{p}\vec{p}$, $\vec{d}\vec{d}$, $\vec{h}\vec{h}$)

Hadron polarimetry requirements for the EIC II

Polarimeters shall determine:

- Bunch polarization profile in x, y, and z
- Polarization lifetime
  - For EIC physics, projection of $\vec{P}$ on stable spin axis required, no in-plane polarization.
- Polarization vector $\vec{P}$ per bunch

Instruments

- Hadron polarimeter (absolute) in IP4
- pC polarimeter (relative) in IP4 and IP6 (between spin rotators)

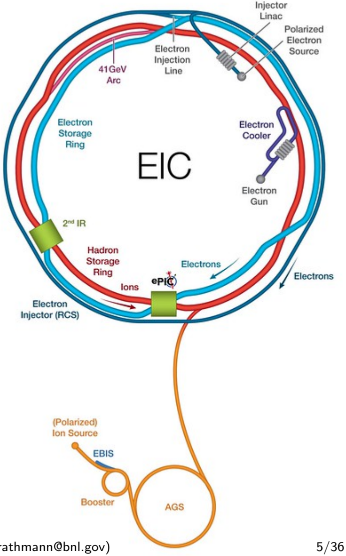

Instruments for absolute and relative polarimetry

Two instruments

- **HJET polarimeter**

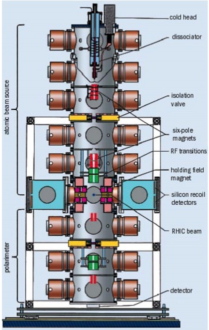

- **absolute, slow**

$$\frac{\Delta P}{P} \approx 3\% \, \text{per} \, 4 \, \text{hour} \qquad (1)$$

- **pC polarimeters**

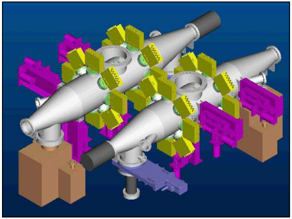

- **fast, relative**

$$\frac{\Delta P}{P} < 1\% \, \text{per scan} \qquad (2)$$

- polarization profile
- polarization lifetime

Absolute polarization from polarized hydrogen jet I

Breit-Rabi polarimeter

- Capable to determine absolute polarization Q of atomic beam, i.e., electron and proton polarization of hydrogen atoms, with accuracy $\Delta Q/Q \lesssim 1\%$.
  - Take this as a given. Will revisit subject through measurements after run 24.
  - At present, no solid estimates available that fully encapsulate BRP systematics at the HJET on the $\approx 1\%$ level.

Beam polarization calibration

1. Proton beam passes through target of polarized H atoms of known polarization Q

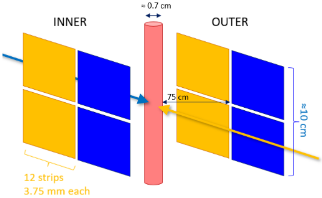

Absolute polarization from polarized hydrogen jet II

Beam polarization calibration

2. Measure number of scattered particles in left (L) and right (R) detectors
3. Sign of Q periodically reversed to compensate for asymmetries caused by differences in detector geometry or efficiency in L and R directions.
4. This determines target asymmetry
$$\epsilon_{\text{target}} = \frac{\text{L} - \text{R}}{\text{L} + \text{R}} = A_y \cdot Q \cos\phi \,. \tag{3}$$
5. Measurement of corresponding asymmetry with beam particles determines ϵ_{beam}. In elastic *pp* scattering, and more general in elastic scattering of *identical* particles, A_y same regardless of which proton is polarized.
6. Absolute beam polarization given by [1–4]
$$\boxed{P = \frac{\epsilon_{\text{beam}}}{\epsilon_{\text{target}}} \cdot Q} \tag{4}$$

Beam-induced target depolarization at RHIC and EIC

Polarized hydrogen jet

- Development of HJET for RHIC finished some 20 yrs ago. Many details on technical structure and development cannot be found in literature. There is no comprehensive publication available
- Refurbishment/upgrades will start after RHIC shutdown (Fall 2025)
- At EIC, bunch repetition frequency much larger than at RHIC $\rightarrow$ **investigate beam-induced depolarization of target and understand situation**

Bunch structure

RHIC situation:

- Time period between two adjacent bunches: $\tau_{\mathrm{b}} = \frac{\tau_{\mathrm{rev}}}{N_b} = 106.57\,\mathrm{ns}$
- Number of stored bunches $N_b = 120$
- Bunch frequency $f_{\mathrm{b}} = \frac{1}{\tau_{\mathrm{b}}} = 9.3831\,\mathrm{MHz}$
- Large number of harmonics contribute to induced magnetic high-frequency field close to RHIC beam, as bunches are short ($\sigma_t \approx 1.8\,\mathrm{ns}$)

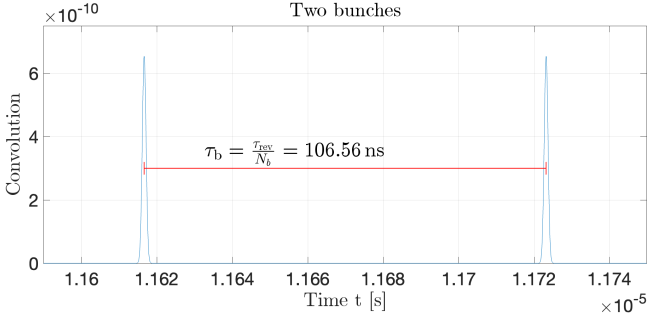

Single bunch distribution

- (Gaussian) bunch in RHIC

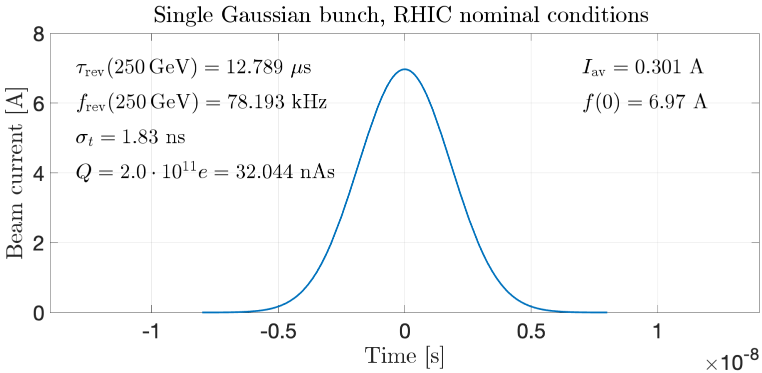

Pulse shape described by

$$f(t) = \frac{Q}{\sqrt{2\,\pi}\sigma_t} \exp\left(-\frac{t^2}{2\sigma_t^2}\right) \tag{5}$$

Gaussian convoluted with (finite) series of delta functions

Total beam current as function of time t given by

$$I(t) = \int_{-\infty}^{\infty} f(t-\xi) \sum_{k=-\infty}^{\infty} \delta\left(\xi - k\frac{\mathcal{T}_{\text{rev}}}{N_{\text{b}}}\right) \mathrm{d}\xi \qquad (6)$$

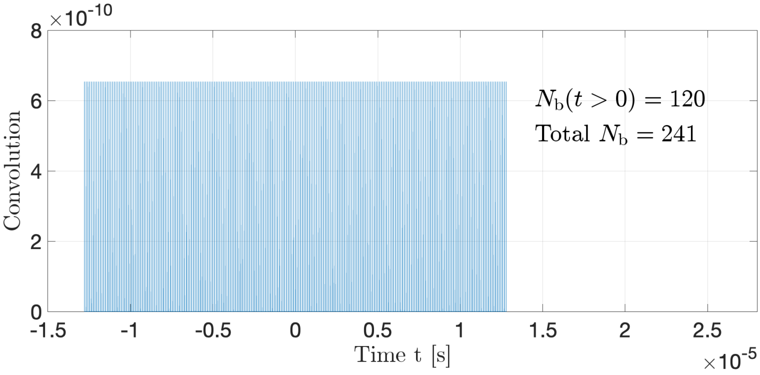

Produced radio-frequency fields

- Single-sided amplitude spectrum of FFT
- x-axis converted to frequency

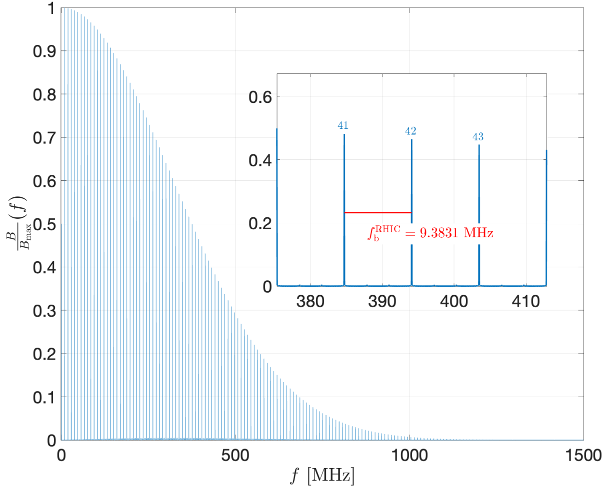

Hyperfine states of hydrogen

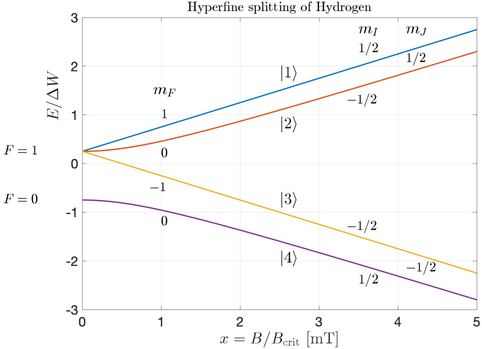

Critical field B_c (see slide 65)

- Zeeman energy $g_J \mu_B B$ comparable to E_{hfs}
- $E_{\mathrm{hfs}} \approx 5.874 \times 10^{-6}$ eV (≈1420 MHz [5]):
- $B_c = 50.7$ mT

Transition frequencies

- Transition frequency between two hyperfine states $|i\rangle$ and $|j\rangle$ given by:

$$f_{ij} = \frac{E_{|i\rangle}(B) - E_{|j\rangle}(B)}{h} \tag{7}$$

- **When f_{ij} matches one of the beam harmonics at a certain holding field $|\vec{B}|$, resonant depolarization occurs** [6–8]

Hyperfine transitions in H from bunch fields at RHIC

Depolarization occurs when f_{ij} multiple of bunch frequency f_b^{RHIC}

- HJET injects states $|1\rangle + |4\rangle$ ($p^{\uparrow}$) and $|2\rangle + |3\rangle$ ($p^{\downarrow}$).
  - What is exact magnitude and orientation of $\vec{B}^{\mathrm{HJET}}$?

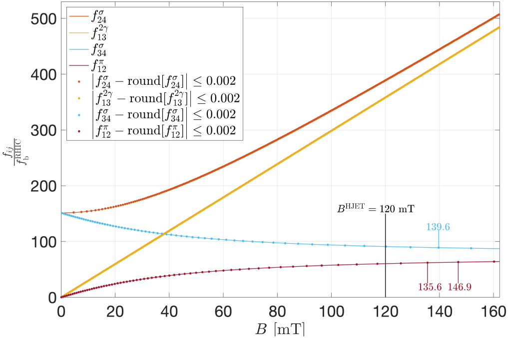

- $\left|\frac{f_{ij}}{f_b^{\mathrm{RHIC}}} - n\right| \le 0.002\,,\; n \in \mathbb{N}$
- No depolarization from same $m_I \Rightarrow f_{14}^{\sigma}$, f_{23}^{π} omitted

HJET at RHIC is operated in safe region around $B_y = 120\,\mathrm{mT}$

- At RHIC, transitions with $\frac{f_{ij}}{f_b^{\mathrm{RHIC}}} \gtrsim 350$ were ignored
- Don't know exactly at which harmonic number, depolarization sets in.

Single bunch distribution

- (Gaussian) bunch in EIC

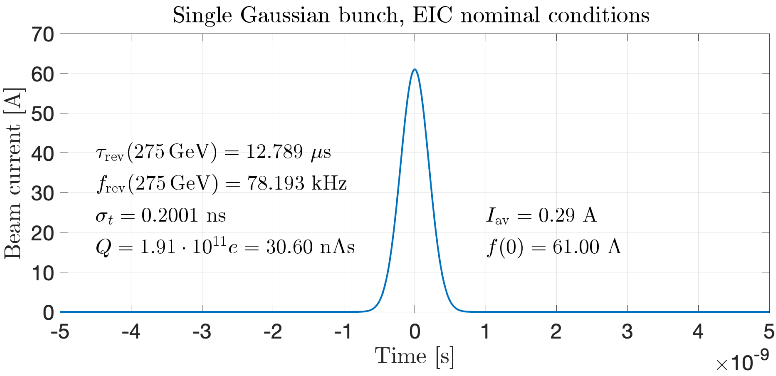

Pulse shape described by

$$f(t) = \frac{Q}{\sqrt{2\pi}\sigma_t} \exp\left(-\frac{t^2}{2\sigma_t^2}\right) \tag{8}$$

Produced radio-frequency fields

- Single-sided amplitude spectrum of FFT

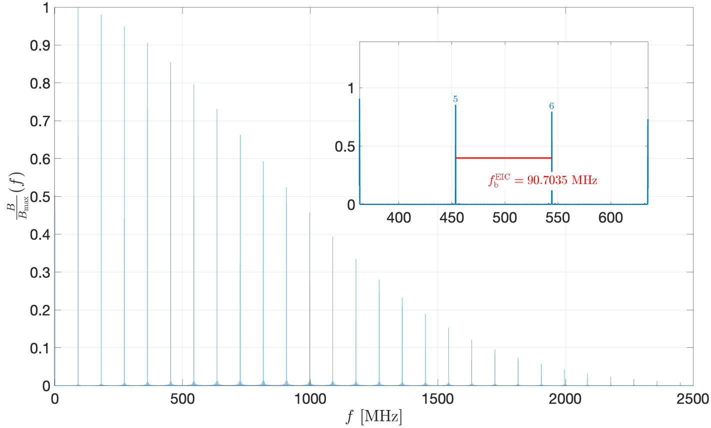

Hyperfine transitions in H from bunch fields at EIC

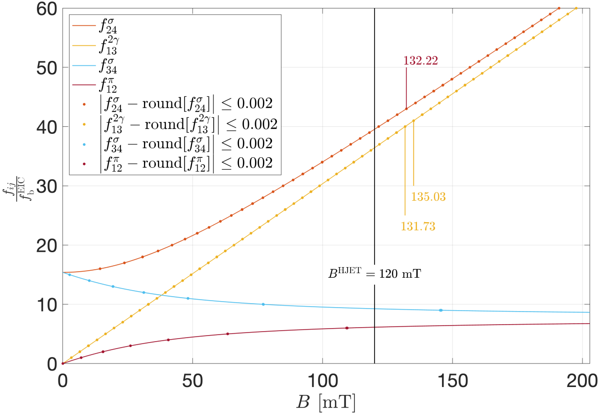

Depolarization (numerically) occurs when $\left|\frac{f_{ij}}{f_b^{\mathrm{EIC}}} - n\right| \leq 0.002\,,\ n \in \mathbb{N}$

In contrast to RHIC, for $B < 200\,\mathrm{mT}$

- **all transitions below harmonic number** ≈ 60 **contribute at EIC!**

Hyperfine transitions in H from bunch fields at EIC

How about the region of small B?

- At RHIC, this region was inaccessible, as spacing of $f_{13}^{2\gamma} \approx 0.3\,\mathrm{mT}$.
- At EIC, at $\approx 5\,\mathrm{mT}$, spacing of $f_{13}^{2\gamma} \approx 3.3\,\mathrm{mT}$.

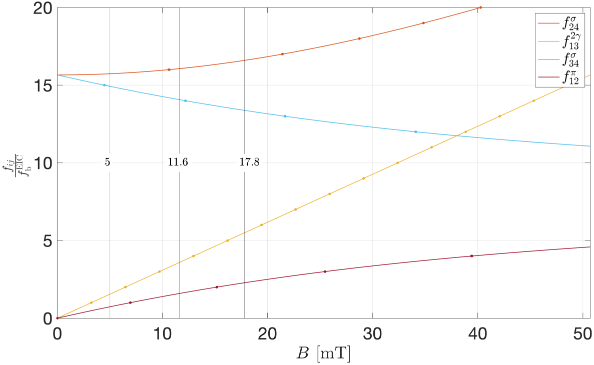

Magnetic field from beam charge

RHIC

Moving charge of beam induces magnetic field at HJET target

- β functions at the HJET in IP12 from G. Robert-Demolaize, 23.07.2024 for RHIC at top energy, determined from fill #34819,

$$\begin{aligned} \beta_x &= 8.243\,\text{m}, \beta_y = 8.326\,\text{m} \\ \beta_x &= 8.303\,\text{m}, \beta_y = 8.252\,\text{m} \end{aligned} \tag{9}$$

- Assume in the following an average $\bar{\beta}_{\text{jet}} = 8.281$
- Since $\beta_x \approx \beta_y$, we deal with a round beam. The normalized RMS emittance taken from the RHIC dashboard during run 24 is:

$$\varepsilon^N_{\text{rms}} = 2.5\,\mu\text{m}\,. \tag{10}$$

Beam parameters for RHIC

- For a Gaussian beam, assume a current density of
$$J = \frac{I(t)}{2\pi\sigma_r^2}\exp\left(-\frac{r^2}{2\sigma_r^2}\right)\,, \quad \text{where} \quad \sigma_r = \sqrt{\frac{\bar{\beta}_{\text{jet}}\epsilon^{\text{N}}_{\text{rms}}}{k\cdot\beta\gamma}} \tag{11}$$
- Due to symmetry of problem, magnetic field $\vec{B}$ will be tangential to concentric circles around z-axis. Thus, $\vec{B}$ can be written as
$$\vec{B} = B(r)\vec{e}_\phi \tag{12}$$
- With beam traveling in $\vec{e}_z$ direction, the integration for a cylindrical Gaussian beam yields flux density
$$\vec{B}(r) = \frac{\mu_0 I(t)}{2\pi r}\left[1-\exp\left(-\frac{r^2}{2\sigma_r^2}\right)\right]\vec{e}_\phi\,, \text{with } \vec{e}_\phi = \vec{e}_z \times \vec{e}_r \tag{13}$$
-

Emittance[2]	Beam width	injection 23.5 GeV	flattop 250 GeV
$\epsilon^N_{\text{rms}} = 2.5\,\mu\text{m}$	$\sigma_r^{1\sigma} = \left(\bar{\beta}_{\text{jet}}\cdot\frac{\epsilon^N_{\text{rms}}}{\beta\gamma}\right)^{\frac{1}{2}}$	0.89 mm	0.28 mm
$\epsilon^N_{95} = \epsilon^N_{\text{rms}}\cdot 5.993$	$\sigma_r^{95} = \sigma_r^{1\sigma}\cdot\sqrt{5.993}$	2.18 mm	0.68 mm

[2] Factor 5.993 to convert 1D rms emittance to emittance for 95% of particles in a beam [9].

Magnetic field from beam charge at RHIC

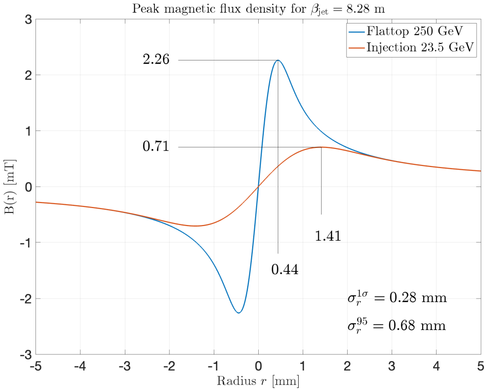

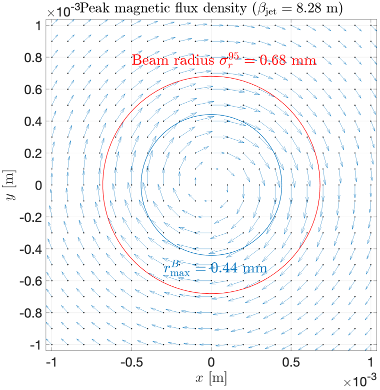

Effect of induced magnetic field on jet pol at RHIC

- Systematic variation of magnetic holding field in region struck by beam

$$\frac{\int_0^{\sigma_r^{95}} B(r)\mathrm{d}r}{\sigma_r^{95}} = 1.73\,\mathrm{mT} \tag{14}$$

- Relative change of target polarization inside beam is, e.g.,

$$\delta P = \frac{P_{|1\rangle+|4\rangle}(\bar{B}^{\mathrm{L}}) - P_{|1\rangle+|4\rangle}(\bar{B}^{\mathrm{R}})}{P_{|1\rangle+|4\rangle}(B_y^{\mathrm{nom}})} \leq 0.21\% \tag{15}$$

Conclusion for RHIC

- No beam-induced depolarization due to variation of B inside beam (slide 15)
- Effect small/tolerable in terms of syst. contribution to jet polarization

Beam parameters

EIC

EIC beam parameters taken from Conceptual Design Report [10]

- 275 GeV
- β-functions:
  - $\beta_x = 230.323\,\text{m}$
  - $\beta_y = 69.935\,\text{m}$
  - $\rightarrow$ assumed in the following: $\bar{\beta} \approx 150\,\text{m}$ for future location of HJET at IP4 (from H. Lovelace, 31.07.2024).
- Like before, $\epsilon_{95}^N = \epsilon_{\text{rms}}^N \cdot 5.993$
- Two situations for IP4:

Beam	ϵ_{rms}^N [µm]	$\sigma_r^{1\sigma}$ [mm]	σ_r^{95} [mm]
uncooled	2.5	1.13	2.76
cooled	0.47	0.49	1.20

Magnetic field from beam charge

EIC

Uncooled beam

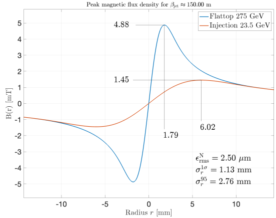

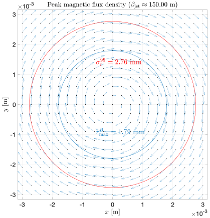

Cooled beam

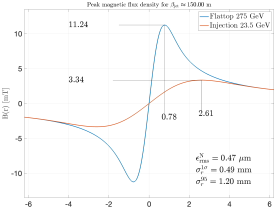

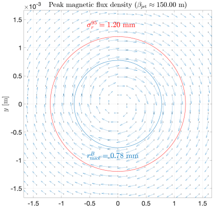

HJET beam size

- On flattop, transverse dimensions of uncooled proton beam at IP4 will be comparable to HJET beam diameter (6 mm FWHM $\rightarrow \sigma^{\mathrm{HJET}} \approx 2.55$ mm).

Effect on magnetic field at jet target and its polarization
EIC

Implications for EIC

1. Induced B field from beam charge:
   - uncooled beam: $B(r) \leq 4.88\,\mathrm{mT}$
   - cooled beam: $B(r) \leq 11.74\,\mathrm{mT}$

   $\rightarrow$ kills idea to apply weak holding field (20 mT) at target (slide 19)
2. Variation of polarization inside target area at 120 mT [Eq. (15)]:
   - uncooled beam: $\delta P = 0.45\%$
   - cooled beam: $\delta P = 1.05\%$
3. **Variation of polarization inside target area at 300 mT [Eq. (15)]:**
   - uncooled beam: $\delta P = 0.1\%$
   - cooled beam: $\delta P = 0.1\%$

Mitigation of beam-induced magnetic field effect at EIC

Possible solutions

1. At RHIC, B-field was moved to $\approx 120\,\text{mT}$ and $\frac{f_{ij}}{f_\text{b}^\text{RHIC}} \geq 350$ ignored (slide 15)
2. **Strategy for EIC: $\Rightarrow$ push harmonics to ≥ 100 $\Rightarrow$ holding field $\geq 350\,\text{mT}$**

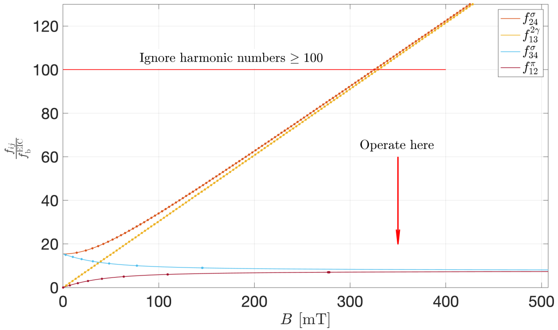

Where exactly is cutoff located for f^σ_{24} and $f^{2\gamma}_{13}$?

- What is know from RHIC or can still be learned about at which B harmonics become harmless?

Holding field system for $|\vec{B}| \approx 0.3\,\mathrm{T}$ with $\vec{B} \parallel \vec{e}_{x,y,z}$

Work together with Helmut Soltner (FZJ, Germany)

Motivation

- Reconcile strong magnetic holding field with open detector geometry to determine all components of beam polarization $\vec{P} = (P_x, P_y, P_z)$ (slide 58)
- Exploit magnetic moments $\vec{m}$ of homogeneously magnetized spheres [11–13]
- Invert $\vec{m}$ in vacuum to reverse $\vec{B}(O)$
- Reorient $\vec{m}$'s to generate $\vec{B}(O) \parallel \vec{e}_{x,y,z}$

Two sets of frames

- Set 1:
  - Interaction region where beam meets atoms at (O)
  - Set 1: $100\,\mathrm{mm}_x \times 100\,\mathrm{mm}_y \times 40\,\mathrm{mm}_z$ and
    Set 2: $100\,\mathrm{mm}_x \times 100\,\mathrm{mm}_y \times 110\,\mathrm{mm}_z$, centered around x, y, and z axes.
  - 8 permanently magnetized spheres in each corner of each frame:
    - NeFeB magnets provide remanence of $B_r = 1.49 - 1.55\,\mathrm{T}$ (type N58)
    - Radius $r = 30\,\mathrm{mm}$

Holding field system: Calculation

- Flux density vector as function of $\vec{m}$ in space

$$\vec{B}(\vec{r}) = \frac{\mu_0}{4\pi}\left[\frac{3\left(\vec{m}\cdot\hat{R}\right)\hat{R} - \vec{m}}{|R|^3}\right] \quad (16)$$

$$\vec{R} = \vec{r} - \vec{r}_0, \hat{R} = \frac{\vec{R}}{|R|}$$

- Optimize orientation of $\vec{m}$'s to maximize $\vec{B}(O)$ in x, y, and z direction:
  - maximize dot product $\vec{m}\cdot\hat{R}$ and set $m_y = 0$, to obtain, e.g., max. B_y.

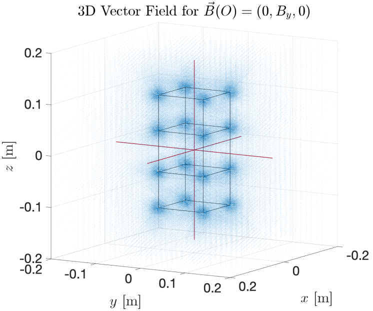

16 magnetized balls

Component $B_{x,y,z}(O)$ using two sets of $\vec{m}$'s

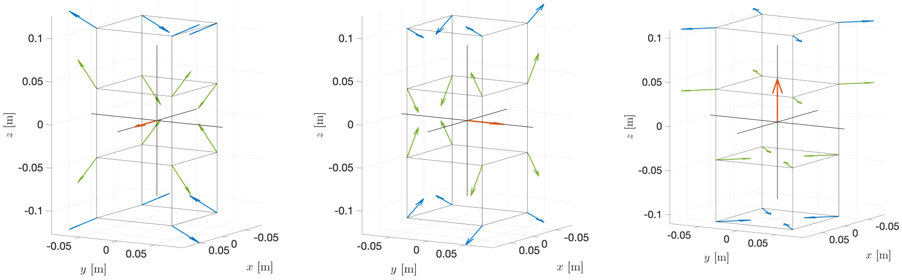

$$B_x: \begin{pmatrix} 0.3224 \\ 0 \\ 0 \end{pmatrix} \mathrm{T} \qquad B_y: \begin{pmatrix} 0 \\ 0.3224 \\ 0 \end{pmatrix} \mathrm{T} \qquad B_z: \begin{pmatrix} 0 \\ 0 \\ 0.3227 \end{pmatrix} \mathrm{T}$$

Technical realization

With properly rotated spheres

- Setup allows for azimuthally symmetric detector setup with acceptance $\Delta\phi \approx \pm 15^\circ$ at $\phi = 45$, 135, 225, and 315°
  - $\phi = \arctan(30/50) = 31^\circ$
- **Technical challenges:**
  1. Accurate 3D reorientation of magnetized spheres[a] in vacuum [14]
  2. Vacuum compatible coatings, like Ni, or stainless steel covers to prevent H and H_2 from deteriorating NeFeB
  3. **First Step: build a lab test setup and verify concept is technically sound**
  4. Forces and torques appear manageable (slide 54)

[a] https://www.youtube.com/watch?v=hhDdfiRCQS4

Polarized $^3\vec{\mathrm{He}}$ Atomic Beam Source (next talk)

Original MIT development for nEDM exp't at Oakridge

- Prajwal T. Mohan Murthy, J. Kelsey, J. Dodge, R. Redwine, R. Milner, P. Binns, B. O'Rourke
- nEDM discontinued

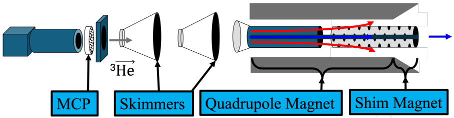

$^3\overrightarrow{\mathrm{He}}$: quadrupole magnet selects spins
- **1.3 K ≈ 86 μeV**
- $\Delta E = \mu_m \approx 67$ neV/T
- initial angle very important

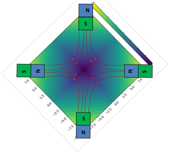

High flux device

- $\simeq 1 \times 10^{14}$ atoms/s $\to d_t \simeq 1 \times 10^{13}$ atoms/cm^2
- an ideal device for absolute $^3\vec{\mathrm{He}}^{++}$ beam polarimetry at EIC

Absolute polarimetry of $\vec{d}$ beams

Dave noted earlier

$\vec{d}$ beams are not part of the EIC baseline

But:

- Atomic beam sources efficiently produce beams of deuterium atoms $\rightarrow$ DJET
- Ideal: use of dual-function RF transition units for $\vec{\mathrm{H}}$ and $\vec{\mathrm{D}}$ atoms
- With vector and tensor polarization accurately determined by BRP, absolute beam polarimetry based on $\vec{d}\vec{d}$ elastic scattering becomes possible
  - $+$ reconstruction of 3D polarization vector, including tensor components.

Polarimetry section at IP4

Carbon, polarized H and ^{3}He gas targets

- Important to set up all polarimeters in one place without much drift, magnetic elements, etc, to minimize spin rotation between them

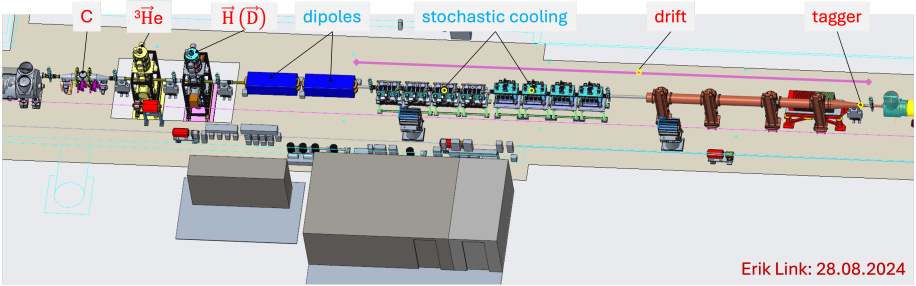

Conclusion

1. Bunch-induced depolarization in H target
   - RHIC: harmonic numbers > 350 were ignored
   - EIC: All depolarizing transitions appear at harmonic numbers < 50
2. Beam-induced magnetic fields perturb target polarization
   - RHIC: Magnetic field involved: $B(r) \leq 2.3\,\mathrm{mT}$
   - EIC: uncooled $B(r) < 4.9\,\mathrm{mT}$
   - EIC: cooled $B(r) < 11.7\,\mathrm{mT}$
   - **Holding field of $|\vec{B}| \geq 300\,\mathrm{mT}$ avoids beam-induced depolarization**
     - **Concept using permanent magnets (NdFeB) appears feasible**
     - **Allows for orientation of holding field $\vec{B}$ in any direction (along x, y, or z)**
3. $^3\vec{\mathrm{He}}$ ABS under development at MIT
   - ideally suited for absolute polarimetry at EIC
   - Polarimetry section in IP4 looks good
4. $\vec{\mathrm{D}}$ and $^3\vec{\mathrm{He}}$ atomic targets at EIC
   - Study bunch-induced depolarization
   - Study beam-induced $\vec{B}$ field effects on target polarizations

Back to my initial observation

- Key issues include funding, talent recruitment, and securing long-term commitment of new partner institutions
- Future of spin physics with $\vec{d}$, ${}^{3}\overrightarrow{\mathrm{He}}^{++}$, or ${}^{6,7}\overrightarrow{\mathrm{Li}}$ beams will no longer even be an option if we wait a few more years to get our act together
- Organize workshops and try to attract groups from national and international scientific community to work on polarization technology

Polarized Ion Sources and Beams at EIC

- **Organizers:** J. Datta, Z.-E. Meziani, R. Milner, D. Raparia, and FR
- **Date:** March 4 – 6, 2025
- **Location:** Stony Brook

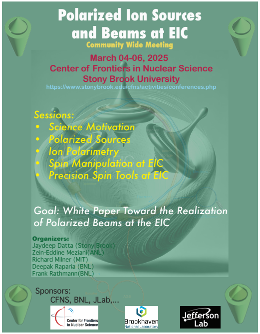

References I

[1] W. Haeberli, "H-jet measures beam polarization at RHIC," CERN Cour. **45N8**, 15 (2005).

[2] I. Nakagawa et al., "RHIC polarimetry," Eur. Phys. J. ST **162**, 259 (2008).

[3] I. G. Alekseev, A. Bravar, G. Bunce, S. Dhawan, K. O. Eyser, R. Gill, W. Haeberli, H. Huang, O. Jinnouchi, A. Kponou, et al., "Measurements of single and double spin asymmetry in *pp* elastic scattering in the cni region with a polarized atomic hydrogen gas jet target," Phys. Rev. D **79**, 094014 (2009), URL `https://link.aps.org/doi/10.1103/PhysRevD.79.094014`.

[4] N. H. Buttimore, "A Helium-3 polarimeter using electromagnetic interference," PoS **PSTP2013**, 057 (2013).

[5] M. Diermaier, C. B. Jepsen, B. Kolbinger, C. Malbrunot, O. Massiczek, C. Sauerzopf, M. C. Simon, J. Zmeskal, and E. Widmann, "In-beam measurement of the hydrogen hyperfine splitting and prospects for antihydrogen spectroscopy," Nature Commun. **8**, 5749 (2017), `1610.06392`.

[6] R. A. Gilman et al., "A Polarized gas internal target using a storage cell in an electron storage ring," Nucl. Instrum. Meth. A **327**, 277 (1993).

[7] A. Airapetian, N. Akopov, Z. Akopov, M. Amarian, A. Andrus, E. Aschenauer, W. Augustyniak, R. Avakian, A. Avetissian, E. Avetissian, et al., "The hermes polarized hydrogen and deuterium gas target in the hera electron storage ring," Nuclear Instruments and Methods in Physics Research Section A: Accelerators, Spectrometers, Detectors and Associated Equipment **540**, 68 (2005), ISSN 0168-9002, URL `https://www.sciencedirect.com/science/article/pii/S0168900204024167`.

[8] K. Ackerstaff et al. (HERMES), "Beam induced nuclear depolarization in a gaseous polarized hydrogen target," Phys. Rev. Lett. **82**, 1164 (1999), `hep-ex/9806006`.

[9] S. Lee, *Accelerator Physics* (World Scientific Publishing Company, 2011), ISBN 9789814405287.

[10] F. Willeke and J. Beebe-Wang, "Electron ion collider conceptual design report 2021," (????), URL `https://www.osti.gov/biblio/1765663`.

References II

[11] P. Blümler and H. Soltner, "Practical Concepts for Design, Construction and Application of Halbach Magnets in Magnetic Resonance," Applied Magnetic Resonance **54**, 1701 (2023), ISSN 1613-7507, URL `https://doi.org/10.1007/s00723-023-01602-2`.

[12] H. Soltner and P. Blümler, "Dipolar halbach magnet stacks made from identically shaped permanent magnets for magnetic resonance," Concepts in Magnetic Resonance Part A **36A**, 211 (2010), `https://onlinelibrary.wiley.com/doi/pdf/10.1002/cmr.a.20165`, URL `https://onlinelibrary.wiley.com/doi/abs/10.1002/cmr.a.20165`.

[13] H. Raich and P. Blümler, "Design and construction of a dipolar halbach array with a homogeneous field from identical bar magnets: Nmr mandhalas," Concepts in Magnetic Resonance Part B: Magnetic Resonance Engineering **23B**, 16 (2004), `https://onlinelibrary.wiley.com/doi/pdf/10.1002/cmr.b.20018`, URL `https://onlinelibrary.wiley.com/doi/abs/10.1002/cmr.b.20018`.

[14] K. Abe, K. Tadakuma, and R. Tadakuma, "Abenics: Active ball joint mechanism with three-dof based on spherical gear meshings," IEEE Transactions on Robotics **37**, 1806 (2021).

[15] N. Akchurin, J. Langland, Y. Onel, B. E. Bonner, M. D. Corcoran, J. Cranshaw, F. Nessi-Tedaldi, M. Nessi, C. Nguyen, J. B. Roberts, et al., "Analyzing power measurement of pp elastic scattering in the coulomb-nuclear interference region with the 200-gev/c polarized-proton beam at fermilab," Phys. Rev. D **48**, 3026 (1993), URL `https://link.aps.org/doi/10.1103/PhysRevD.48.3026`.

[16] N. Ramsey, *Molecular Beams* (Oxford University Press, 1956).

[17] F. Rathmann et al., "Complete angular distribution measurements of pp spin correlation parameters Axx, Ayy, and Axz and analyzing power Ay at 197.4 MeV," Phys. Rev. C **58**, 658 (1998).

References III

[18] B. von Przewoski et al., "Proton proton analyzing power and spin correlation measurements between 250-MeV and 450-MeV at $7^\circ \leq \theta(c.m.) \leq 90^\circ$ with an internal target in a storage ring," Phys. Rev. C **58**, 1897 (1998).

[19] B. von Przewoski, H. O. Meyer, P. V. Pancella, S. F. Pate, R. E. Pollock, T. Rinckel, F. Sperisen, J. Sowinski, W. Haeberli, W. K. Pitts, et al., "Absolute measurement of the p+p analyzing power at 183 mev," Phys. Rev. C **44**, 44 (1991), URL https://link.aps.org/doi/10.1103/PhysRevC.44.44.

[20] G. Plattner and A. Bacher, "Absolute calibration of spin-$\frac{1}{2}$ polarization," Physics Letters B **36**, 211 (1971), ISSN 0370-2693, URL https://www.sciencedirect.com/science/article/pii/0370269371900712.

[21] B. v. Przewoski et al., "Analyzing powers and spin correlation coefficients for $p + d$ elastic scattering at 135 and 200 MeV," Phys. Rev. C **74**, 064003 (2006), URL http://link.aps.org/doi/10.1103/PhysRevC.74.064003.

[22] R. E. Pollock, W. A. Dezarn, M. Dzemidzic, J. Doskow, J. G. Hardie, H. O. Meyer, B. v. Przewoski, T. Rinckel, F. Sperisen, W. Haeberli, et al., "Calibration of the polarization of a beam of arbitrary energy in a storage ring," Phys. Rev. E **55**, 7606 (1997), URL https://link.aps.org/doi/10.1103/PhysRevE.55.7606.

Spare slides

Radiofrequency-fields

FFT of convolution

- Two-sided amplitude spectrum of FFT of the convolution

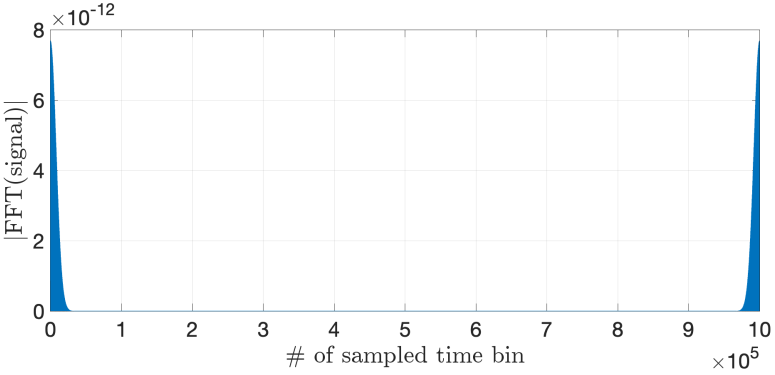

Amplitudes of magnetic RF fields

- Same, but logy
- FFT background $\leq 1\%$
  - not at f_{rev}
  - not from finite set of δ fcts
  - $\rightarrow$ probably numerical from FFT

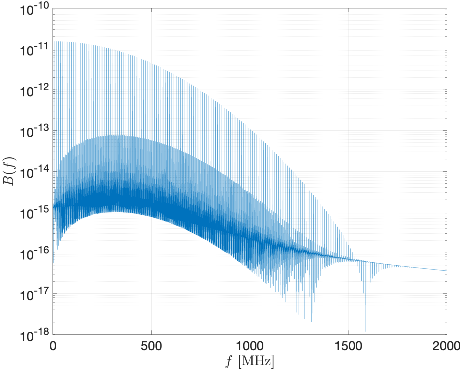

Asymmetry and polarization

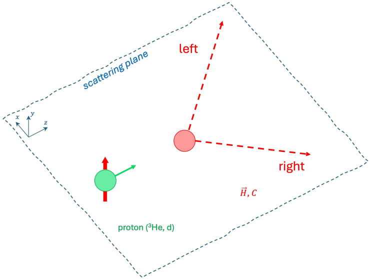

- Spin-dependent cross section

$$\sigma = \sigma_0(1 + A_y P_y \cos\phi) \qquad (17)$$

  - Unpolarized cross section σ_0
  - P_y vertical component of beam polarization $\vec{P} = (P_x, P_y, P_z)$
  - Analyzing power $A_y = \frac{\sigma^{\text{left}} - \sigma^{\text{right}}}{\sigma^{\text{left}} + \sigma^{\text{right}}}$
  - Azimuth of scattered particle ϕ

Coulomb-nuclear interference (CNI)

- A_y: measure of polarization sensitivity of scattering process
- **At AGS and RHIC energies, no scattering processes available with A_y known to sufficient accuracy for $\Delta P \leq 0.01$ [1].**
- **Interference of EM and strong interaction at small scattering angles provides sizable analyzing power for elastic *pp* (and *pN*) scattering.**

Coulomb-Nuclear interference I

Need for calibration

- Asymmetry from CNI region constitutes basis of RHIC high-energy (absolute) polarimeters
  - derived from same EM amplitude that generates anomalous magnetic moment

$$\mu_p = g_p \frac{e\hbar}{2m_p} = g_p \mu_N, \quad g_p \approx 5.585$$
$$g_p - 2 \approx 3.585 \Rightarrow \mu_p^{\text{anomalous}} \approx 1.792\, \mu_N \tag{18}$$

  - E704 at Fermilab used 200 GeV/c $\vec{p}$ from hyperon decay to detect asymmetry in scattering from H target [15]. Largest $A_y \approx 0.04$ with large statistical errors.
  - Meanwhile, accurate measurements of A_y are available from RHIC [3]
- Asymmetry measurements involve normalization uncertainties and calculations of A_y are subject to uncertainties in amplitudes of strong interaction. **Therefore, accurate calibration of reaction required.**

Coulomb-Nuclear interference II

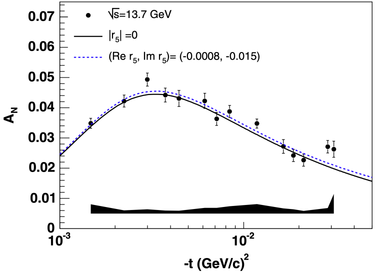

Measured A_N from RHIC in the CNI region at $\sqrt{s} = 6.8\,\mathrm{GeV}$ ($E_{\mathrm{lab}} = 23.7\,\mathrm{GeV}$) [3].

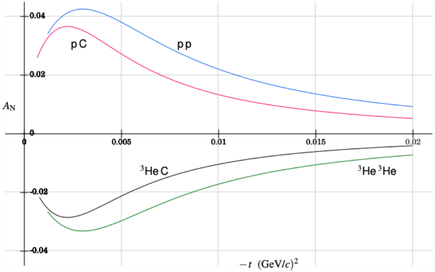

Calculation of A_y in the CNI region by Nigel Buttimore [4].

Detector system at the polarized jet target

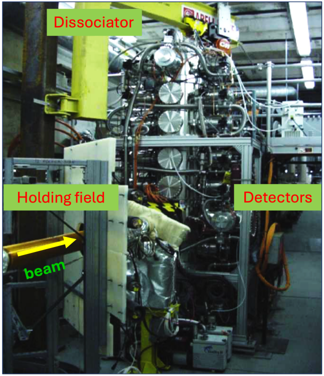

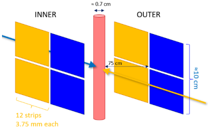

Eight Si strip detect.

- 12 vertical strips
- 3.75 mm pitch
- 500 μm thickness

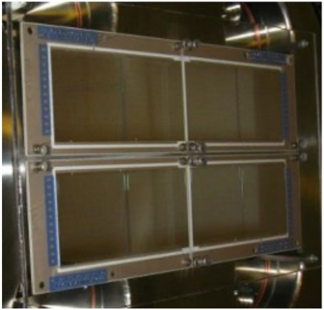

With present setup of L-R detectors and guide field B_y

- Only vertical component P_y measurable via L-R asymmetry near $\theta = 90^\circ$.

CNI polarimeter setup

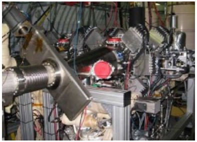

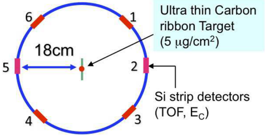

CNI setup with 6 Si detectors at different azimuth at each target enables

- determination of polarization components P_x and P_y
- determination of polarization profile along x and y
- Due to parity violation, $A_z \approx 0$ (no longitudinal analyzing power) $\rightarrow P_z$ not measurable with *unpolarized* target

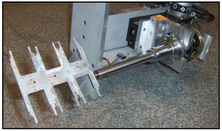

Ultra-thin ribbon targets

- 8 target holder inside beam pipe
- 2 holders per beam for x and y
- 6 targets per holders, 48 in total
- Targets $\approx 10\,\mu\text{m} \times 100\,\text{nm}$, hand crafted by D. Steski & team

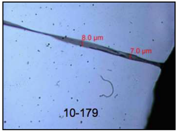

Bunch structure

EIC situation:

- Time period between two adjacent bunches: $\tau_\mathrm{b} = \frac{\tau_\mathrm{rev}}{N_b} = 10.85\,\mathrm{ns}$
- Number of stored bunches $N_b = 1160$
- Bunch frequency $f_\mathrm{b} = \frac{1}{\tau_\mathrm{b}} = 92.2081\,\mathrm{MHz}$

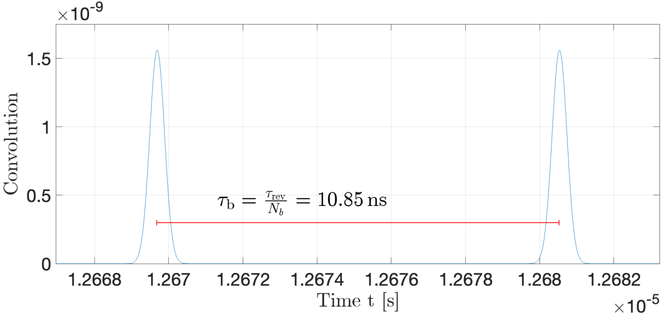

Transition frequencies between hyperfine states of H

Based on Zeeman splitting (slide 14) using Eq. (7)

- Determine transition frequencies f_{ij} between hyperfine states $|i\rangle$ and $|j\rangle$.
- Classification refers to change of quantum numbers (see Ramsey [16]):
  - B_0 is static field, B_1 is RF field that exerts torque on magnetic moment μ:
  - π ($B_1 \perp B_0$) transitions *within one* F multiplet:

$$\Delta F = 0, \quad \Delta m_F = \pm 1. \tag{19}$$

  - σ ($B_1 \parallel B_0$) transitions *between different* F multiplets:

$$\Delta F = \pm 1, \quad \Delta m_F = 0, \pm 1. \tag{20}$$

Possible transitions

- Single photon transitions in H: f_{12}^{π}, f_{23}^{π}, f_{14}^{σ}, f_{24}^{σ}, and f_{34}^{σ}.
- Transition $f_{13}^{2\gamma}$ with $\Delta m_F = 2$ requires two photons.

Amplitudes of radio-frequency fields

- Frequency spacing becomes larger at EIC $\Rightarrow$ fewer resonances contribute
- RF field amplitudes at EIC $\approx 10\times$ larger compared to RHIC
  $\Rightarrow$ increased transition probability due more photons ($n_\gamma \propto B^2$).

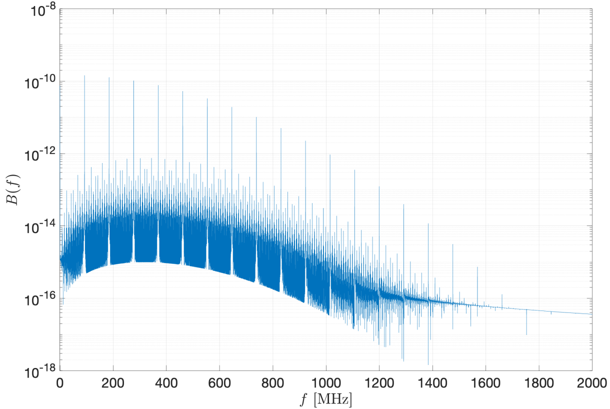

Gaussian convoluted with (finite) series of delta functions

Total beam current as function of time t given by

$$I(t) = \int_{-\infty}^{\infty} f(t-\xi) \sum_{k=-\infty}^{\infty} \delta\left(\xi - k\frac{T_{\mathrm{rev}}}{N_{\mathrm{b}}}\right) \mathrm{d}\xi \tag{21}$$

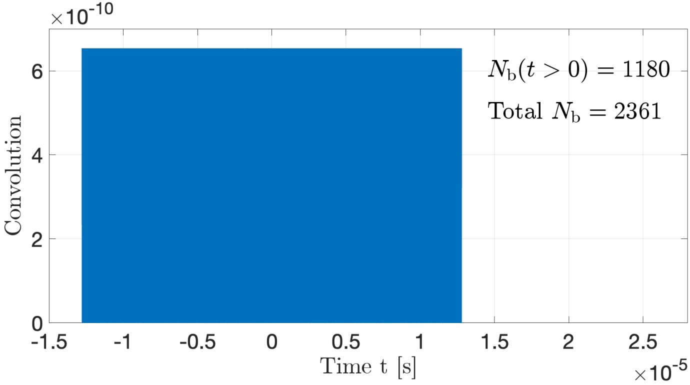

Transition frequencies between hyperfine states of H

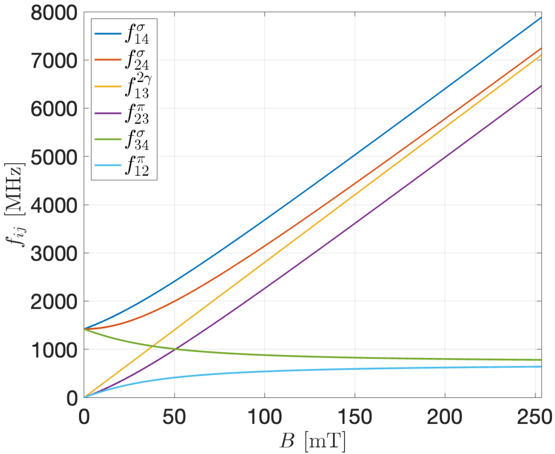

For $n = 4$ hyperfine states, $\binom{n}{2} = 6$ transitions possible.

Magnetic field from beam charge

EIC

Cooled beam

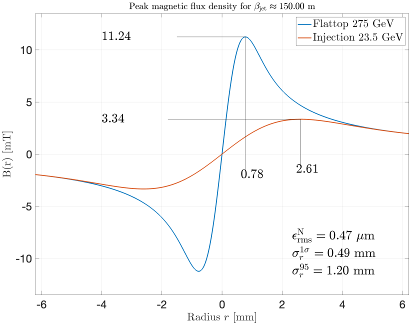

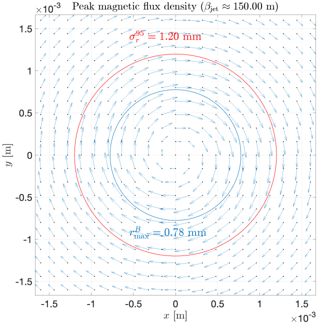

Force and torque between two dipoles $\vec{m}_1$ and $\vec{m}_2$ I

Potential energy of magnetic dipole

$$
\begin{aligned}
U &= -\vec{m}\cdot\vec{B} \\
\vec{F} = -\vec{\nabla}U \quad &\rightarrow \quad F_{12} = \vec{\nabla}\left(\vec{m}_2\cdot\vec{B}_1\right)
\end{aligned}
\tag{22}
$$

- $\vec{B}_1$ is flux density produced by $\vec{m}_1$ at location of $\vec{m}_2$.

Force:

$$
\begin{aligned}
\vec{F}_{12}(\vec{r}_{12},\vec{m}_1,\vec{m}_2) = \frac{3\mu_0}{4\pi r_{12}^4}\Big[&\vec{m}_2\left(\vec{m}_1\cdot\vec{e}_{12}\right)+\vec{m}_1\left(\vec{m}_2\cdot\vec{e}_{12}\right)+\vec{e}_{12}\left(\vec{m}_1\cdot\vec{m}_2\right) \\
&-5\vec{e}_{12}\left(\vec{m}_1\cdot\vec{e}_{12}\right)\left(\vec{m}_2\cdot\vec{e}_{12}\right)\Big]
\end{aligned}
\tag{23}
$$

- $\vec{r}_{12}$ is vector between $\vec{m}_1$ and $\vec{m}_2$, $\vec{e}_{12} = \frac{\vec{r}_{12}}{|r_{12}|}$.

Torque

$$
\vec{\tau} = \vec{m}_2\times\vec{B}_1 \tag{24}
$$

Force and torque between two dipoles $\vec{m}_1$ and $\vec{m}_2$ II

Examples: $\vec{m}_1 \perp \vec{m}_2$

1. Spheres touch:

$$r_{12} = 0.06\,\mathrm{m} \quad \vec{F}_{12} = -417\,\mathrm{N} \quad \tau_{12} = 8.3\,\mathrm{Nm} \tag{25}$$

2. System assembled:

$$r_{12} \geq 0.07\,\mathrm{m} \quad \vec{F}_{12} \leq -225\,\mathrm{N} \quad \tau_{12} = 5.2\,\mathrm{Nm} \tag{26}$$

Flux density of system in 3D

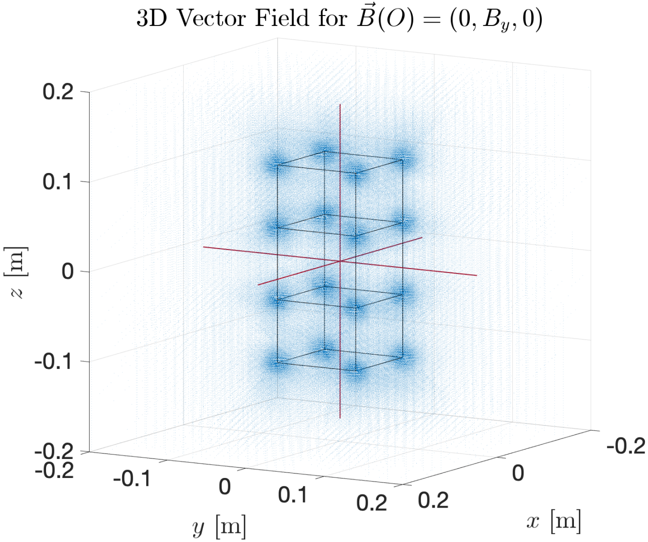

No zero crossings along axes

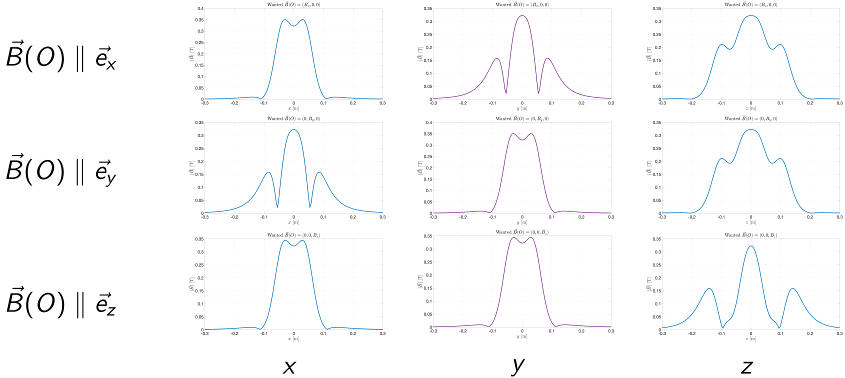

- No zero crossing of magnetic field along vertical jet (y) axis
- $B_y^{\text{min}} \approx 1.9\,\text{mT}$ sufficient to avoid Majorana depolarization
- Field integrals along beam (z) axis

$\vec{B}(O)$	$\parallel \vec{e}_x$	$\parallel \vec{e}_y$	$\parallel \vec{e}_y$
$\int \lvert\vec{B}\rvert \mathrm{d}z$	$0.0667\,\text{Tm}$	$0.0667\,\text{Tm}$	$0.0546\,\text{Tm}$

Concept for magnetic guide field for HJET at EIC

Spin-dependent pp elastic cross section (spin 1/2 + spin 1/2)

With polarized beam $\vec{P}$ and polarized target $\vec{Q}$, all components of $\vec{P}$ can be determined from spin-dependent cross section, as shown in Table below [17, 18]:

$$
\begin{aligned}
\sigma/\sigma_0 = 1 &+ A_y \left[(P_y + Q_y)\cos\phi - (P_x + Q_x)\sin\phi\right] \\
&+ A_{xx}\left[P_x Q_x \cos^2\phi + P_y Q_y \sin^2\phi + (P_x Q_y + P_y Q_x)\sin\phi\cos\phi\right] \\
&+ A_{yy}\left[P_x Q_x \sin^2\phi + P_y Q_y \cos^2\phi - (P_x Q_y + P_y Q_x)\sin\phi\cos\phi\right] \\
&+ A_{xz}\left[(P_x Q_z + P_z Q_x)\cos\phi + (P_y Q_z + P_z Q_y)\sin\phi\right] + A_{zz} P_z Q_z
\end{aligned}
$$

- Full angular distributions of all A_{ik}'s were determined.
- Single input: $A_y = 0.2122 \pm 0.0017$ at $\theta_{\mathrm{lab}} = 8.64^\circ \pm 0.07^\circ$ [19], known from $A_y = 1$ point in $p + {}^{12}\mathrm{C}$ elastic scattering [20].

Most importantly in context

- determination of beam $\vec{P} = (P_x, P_y, P_z)$ and target $\vec{Q} = (Q_x, Q_y, Q_z)$, as well as non-flipping components possible (slide 68)

Spin-dependent *pp* elastic cross section

The above is relevant for two reasons

1. The spin-dependence of $\vec{p}\vec{p}$ elastic scattering allows to reconstruct angular distributions of all (in that case five) polarization observables.
2. With suitable magnetic guide field, target polarization $\vec{Q}$ can be oriented along any direction, for instance along x, so that $\vec{Q} = Q \cdot \vec{e}_x = \vec{Q}_x$
   - Absolute value of target polarization Q determined by BRP

Two things needed to port HJET from RHIC to EIC with $\frac{\Delta P}{P} \leq 1\%$

1. Substantially stronger holding field of $|\vec{B}| \approx 300$ to $350\,\mathrm{mT}$ than at RHIC
2. Detector capable to pick up azimuthal asymmetries $\propto \sin\phi$ and $\propto \sin 2\phi$ (slide 67)
   - foresee proper detector symmetry to provide $\vec{d}\vec{d}$ beam absolute polarimetry, i.e., beyond $\propto \sin 2\phi$.

Will carbon fiber targets survive at EIC?

Target heating calculated according to Peter Thieberger

- With proper beam sizes, there is not much difference between RHIC and EIC.
- But, RF heating of the targets not included, will be more severe at EIC due to shorter bunches.
- RF design of target holders needs to be optimized.

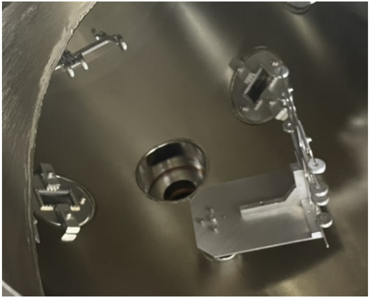

Carbon target temperatures from Thieberger's estimate

RHIC typical conditions

- 250 GeV
- 111 bunches
- 16×10^{10} protons per bunch
- $\sigma_r^{95} = 0.68\,\mathrm{mm}$

TARGET	GRAPHITE	TUNGSTEN	CARBON
Density (g/cc)	2.26	19.3	2.26
LET (MeV cm^2/g)	1.76E-03	1.12E-03	6.33E-04
Thermal conductivity [W/(K * m)]	390	173	390
Emissivity	0.8	0.35	0.8
Specific heat (J/ (gm K)	0.72	0.134	0.72
Thickness (nm)	50	100	50
Sublimation or melting limit (°C)	2227	3422	2227

PROTON BEAM	RHIC 2017	EIC	XX bunch
Beam rms width (mm)	0.68	1.2	
# of protons per bunch	1.60E+11	6.90E+10	
# of bunches	111	1160	

Thermal conductivity multiplier	1
Simulation time step (ns)	500

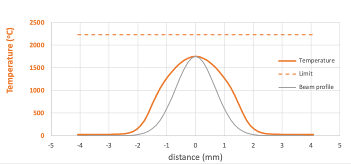

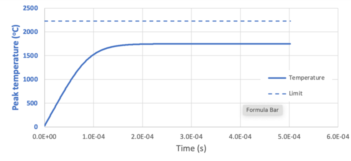

Carbon target temperatures from Thieberger's estimate

EIC for highest luminosity

- 275 GeV
- 1160 bunches
- 6.9×10^{10} protons per bunch
- $\sigma_r^{95} = 1.2\,\text{mm}$ **cooled beam** (slide 21)

TARGET	GRAPHITE	TUNGSTEN	CARBON
Density (g/cc)	2.26	19.3	2.26
LET (MeV cm^2/g)	1.76E-03	1.12E-03	6.33E-04
Thermal conductivity [W/(K * m)]	390	173	390
Emissivity	0.8	0.35	0.8
Specific heat (J/ (gm K)	0.72	0.134	0.72
Thickness (nm)	50	100	50
Sublimation or melting limit (°C)	2227	3422	2227

PROTON BEAM	RHIC 2017	EIC	XX bunch
Beam rms width (mm)	0.68	1.2	
# of protons per bunch	1.60E+11	6.90E+10	
# of bunches	111	1160	

Thermal conductivity multiplier	1
Simulation time step (ns)	500

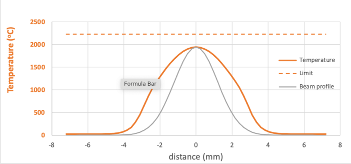

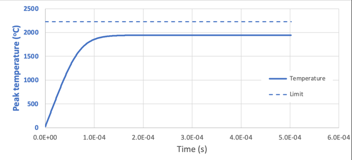

Carbon target temperatures from Thieberger's estimate

EIC for highest luminosity

- 275 GeV
- 1160 bunches
- 6.9×10^{10} protons per bunch
- $\sigma_r^{95} = 2.8\,\text{mm}$ **uncooled beam** (slide 24)

TARGET	GRAPHITE	TUNGSTEN	CARBON
Density (g/cc)	2.26	19.3	2.26
LET (MeV cm^2/g)	1.76E-03	1.12E-03	6.33E-04
Thermal conductivity [W/(K * m)]	390	173	390
Emissivity	0.8	0.35	0.8
Specific heat (J/ (gm K)	0.72	0.134	0.72
Thickness (nm)	50	100	50
Sublimation or melting limit (°C)	2227	3422	2227

PROTON BEAM	RHIC 2017	EIC	XX bunch
Beam rms width (mm)	0.68	2.8	
# of protons per bunch	1.60E+11	6.90E+10	
# of bunches	111	1160	

Thermal conductivity multiplier	1
Simulation time step (ns)	500

Formula Bar

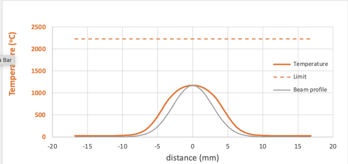

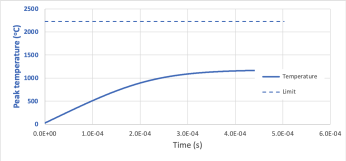

Direct measurement of target temperature

Direct determination of target temperature

- measurement of visible and infrared light
- present light-collecting lens badly aligned on C target interaction region
  - C target chamber already pumped down when equipment became available
  - Need dedicated APEX next year to align with *open* C target chamber
  - Calibration of signal temperature using 1:1 lab setup at 2500 K oven


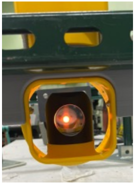


Critical field for hydrogen hyperfine splitting I

Zeeman region:

- magnetic flux density at which energy separation between different hyperfine levels becomes comparable to Zeeman splitting.
- referred to as *critical magnetic field* or *Breit-Rabi field* B_c
- Breit-Rabi formula (energy levels of hydrogen atom in external magnetic field:

$$E_{F,m_F} = -\frac{E_{\mathrm{hfs}}}{2(2I+1)} + g_J \mu_B m_J B \pm \frac{E_{\mathrm{hfs}}}{2}\sqrt{1 + \frac{2m_F x}{F} + x^2}\,,\text{where} \qquad (27)$$

- E_{hfs} is hyperfine splitting energy
- I is nuclear spin (for H, $I = \frac{1}{2}$)
- g_J is Landé g-factor
- μ_B is Bohr magneton
- m_J is magnetic quantum number
- m_F is total angular momentum quantum number
- $x = \frac{g_J \mu_B B}{E_{\mathrm{hfs}}}$
- $F = I + J$ is total angular momentum (for H, $J = \frac{1}{2}$)

Critical field for hydrogen hyperfine splitting II

For H:

- hyperfine splitting energy $E_{\rm hfs}$ (1420 MHz):
$$E_{\rm hfs} \approx 5.874 \times 10^{-6}\,\mathrm{eV} \tag{28}$$
- Critical field B_c is when Zeeman energy $g_J \mu_B B$ is comparable to $E_{\rm hfs}$. With $g_J \mu_B B_c \approx E_{\rm hfs}$, we get:
$$B_c \approx \frac{E_{\rm hfs}}{g_J \mu_B} \tag{29}$$
- For H, $g_J \approx 2$ (approximately for electron), and $\mu_B \approx 5.788 \times 10^{-5}\,\mathrm{eV/T}$. Thus,
$$B_c \approx \frac{5.874 \times 10^{-6}\,\mathrm{eV}}{2 \times 5.788 \times 10^{-5}\,\mathrm{eV/T}} \approx 50.7\,\mathrm{mT} \tag{30}$$

Detector symmetry required to accomplish the task

For spin $\frac{1}{2}$ + spin $\frac{1}{2}$ scattering, suitable geometry below shows pattern of detected azimuthal angles [17].

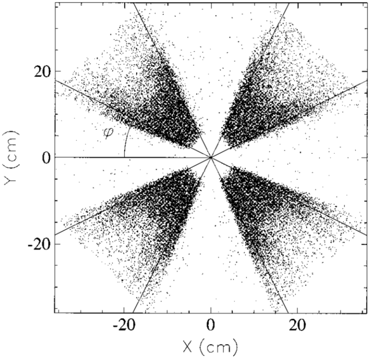

For spin $\frac{1}{2}$ + spin 1 scattering, a higher segmentation is needed, because besides $\sin\phi$ and $\sin 2\phi$, also terms $\sin 3\phi, \ldots$ contribute to asymmetries [21].

Polarization of beam $\vec{P}$ and target $\vec{Q}$ [17, 18]

	$\pm x$		$\pm y$		$\pm z$	
	PRE	POST	PRE	POST	PRE	POST
P_x	0.0052(47)	0.0089(44)	0.0052(47)	0.0089(44)	0.0052(47)	0.0089(44)
P_y [a]	**0.5801(34)**	**0.5425(32)**	**0.5802(34)**	**0.5417(32)**	**0.5765(34)**	**0.5447(32)**
P_z	−0.0021(47)	0.0003(44)	−0.0021(47)	0.0003(44)	−0.0021(47)	0.0003(44)
Q_x	**0.7401(59)**	**0.7394(56)**	−0.0039(59)	0.0039(56)	−0.0071(23)	−0.0052(23)
Q_y	0.0111(59)	0.0039(56)	**0.7400(59)**	**0.7406(56)**	−0.0055(59)	−0.0034(56)
Q_z	0.0158(60)	0.0240(60)	−0.0174(61)	−0.0121(61)	**0.7401(42)** [b]	**0.7400(40)** [b]
S_{P_y}	−0.0008(18)	−0.0005(17)	−0.0008(18)	0.0005(17)	−0.0008(18)	0.0005(17)
S_{Q_x}	0.0017(23)	−0.0007(23)	−0.0040(23)	−0.0031(23)	−0.0043(23)	−0.0024(23)
S_{Q_z}	−0.0091(82)	−0.0162(82)	−0.0177(82)	−0.0197(82)	0.0013(82)	−0.0086(82)

- Beam polarization export/calibration to arbitrary energy [22]

  - PRE $\equiv$ b (197.4 MeV)
  - Export $\equiv$ c (399.1 MeV)
  - POST $\equiv$ d (197.4 MeV)